Am J Physiol Heart Circ Physiol 302: H1625–H1635, 2012.
First published February 3, 2012; doi:10.1152/ajpheart.00960.2011.

Electromechanical and structural alterations in the aging rabbit heart and aorta

Leroy L. Cooper,[1,2]* Katja E. Odening,[1]* Min-Sig Hwang,[3,4] Leonard Chaves,[1] Lorraine Schofield,[1] Chantel A. Taylor,[1] Anthony S. Gemignani,[5] Gary F. Mitchell,[6] John R. Forder,[3,7] Bum-Rak Choi,[1] and Gideon Koren[1]

[1]*Cardiovascular Research Center,* [5]*Division of Cardiology, Rhode Island Hospital, Warren Alpert Medical School of Brown University, Providence;* [2]*Department of Molecular Pharmacology, Physiology, and Biotechnology, Brown University, Providence;* [7]*Department of Radiology,* [4]*Department of Neuroscience,* [3]*McKnight Brain Institute, University of Florida, Gainesville; and* [6]*Cardiovascular Engineering, Incorporated, Norwood, Massachusetts*

Submitted 29 September 2011; accepted in final form 27 January 2012

Cooper LL, Odening KE, Hwang MS, Chaves L, Schofield L, Taylor CA, Gemignani AS, Mitchell GF, Forder JR, Choi BR, Koren G. Electromechanical and structural alterations in the aging rabbit heart and aorta. *Am J Physiol Heart Circ Physiol* 302: H1625–H1635, 2012. First published February 3, 2012; doi:10.1152/ajpheart.00960.2011.— Aging increases the risk for arrhythmias and sudden cardiac death (SCD). We aimed at elucidating aging-related electrical, functional, and structural changes in the heart and vasculature that account for this heightened arrhythmogenic risk. Young (5–9 mo) and old (3.5–6 yr) female New Zealand White (NZW) rabbits were subjected to in vivo hemodynamic, electrophysiological, and echocardiographic studies as well as ex vivo optical mapping, high-field magnetic resonance imaging (MRI), and histochemical experiments. Aging increased aortic stiffness (baseline pulse wave velocity: young, 3.54 ± 0.36 vs. old, 4.35 ± 0.28 m/s, $P < 0.002$) and diastolic (end diastolic pressure-volume relations: 3.28 ± 0.5 vs. 4.95 ± 1.5 mmHg/ml, $P < 0.05$) and systolic (end systolic pressure-volume relations: 20.56 ± 4.2 vs. 33.14 ± 8.4 mmHg/ml, $P < 0.01$) myocardial elastances in old rabbits. Electrophysiological and optical mapping studies revealed age-related slowing of ventricular and His-Purkinje conduction (His-to-ventricle interval: 23 ± 2.5 vs. 31.9 ± 2.9 ms, $P < 0.0001$), altered conduction anisotropy, and a greater inducibility of ventricular fibrillation (VF, 3/12 vs. 7/9, $P < 0.05$) in old rabbits. Histochemical studies confirmed an aging-related increased fibrosis in the ventricles. MRI showed a deterioration of the free-running Purkinje fiber network in ventricular and septal walls in old hearts as well as aging-related alterations of the myofibrillar orientation and myocardial sheet structure that may account for this slowed conduction velocity. Aging leads to parallel stiffening of the aorta and the heart, including an increase in systolic stiffness and contractility and diastolic stiffness. Increasingly, anisotropic conduction velocity due to fibrosis and altered myofibrillar orientation and myocardial sheet structure may contribute to the pathogenesis of VF in old hearts. The aging rabbit model represents a useful tool for elucidating age-related changes that predispose the aging heart to arrhythmias and SCD.

cardiac electrophysiology; cardiac hemodynamics; optical mapping; high-field magnetic resonance imaging

AGING IS ASSOCIATED WITH AN increased incidence of cardiac arrhythmias and is a known independent risk factor for sudden cardiac death (SCD) (22). Multiple factors may influence age-related SCD, including structural and electrical changes in the heart. Aging results in increased fibrosis and reduced cellular coupling in the cardiac muscle (14, 45) and the specialized conduction system (18), which slows activation and conduction velocity (CV) throughout both the ventricle (13) and the His-Purkinje system (16, 18, 48, 55). Age-related alterations in anisotropic CV with a preferentially reduced transverse conduction provide a substrate for reentrant arrhythmias and exert a proarrhythmic effect by decreasing the threshold for ventricular fibrillation (VF) in various animal models of aging, such as rabbits, dogs, and mice (13, 25, 53, 54).

In addition to direct electrophysiological effects, the effects of aging on cardiac mechanical function and vascular structure may contribute to increased arrhythmogenic risk. Indeed, it is known that, in humans, aging is associated with increased arterial stiffness and pulse pressure, which are associated with an increased susceptibility to various cardiac events, including arrhythmia (33, 34, 38).

In light of the many environmental confounders associated with aging in humans, elucidation of major causes and underlying mechanisms of SCD has proven difficult. Studies in humans generally provide only statistical associations (47, 61), which require subsequent validation in experimental models for a more thorough examination of the causal relations between aging and increased incidence of SCD. It is known that the rabbit's action potential shape and its ionic composition are similar to humans (46, 57). Hence, we examined aging-related changes in cardiac electrophysiological, mechanical, and structural features in a rabbit model, and we also related sequelae of vasculature aging to structural and electrophysiological alterations in the myocardium, thereby providing a more thorough assessment of pathophysiological alterations that may render the aging heart more susceptible to arrhythmia and SCD.

METHODS

Animal Ethical Statement

All animal studies were performed in accordance with the local guidelines of the institutions and only after approval by the Institutional Animal Care and Use Committee in accordance with the *Guide for the Care and Use of Laboratory Animals* published by the United States National Institutes of Health (NIH Publication no. 85–23, revised 1996).

Aortic Pullback and Pulse Wave Velocity

Pulse wave velocity (PWV) was assessed via aortic pullback as previously described (36, 37). Briefly, under fluoroscopic guidance, a 3-Fr dual pressure-volume catheter (Millar Instruments, Houston, TX) was inserted through a 3-Fr sheath via the right carotid artery and advanced to the proximal aorta. Additionally, a 2-Fr pressure catheter (Millar Instruments) was inserted via the femoral artery and advanced retrogradely to the proximal aorta. An incremental 10-cm pullback of

* L. L. Cooper and K. E. Odening contributed equally to this work.

Address for reprint requests and other correspondence: G. Koren, Cardiovascular Research Center, Rhode Island Hospital, Brown Univ. School of Medicine, 1 Hoppin St., West Coro-5, Providence, RI 02903 (e-mail: Gideon_Koren@Brown.edu).

the femoral pressure catheter was performed, with proximal and distal pressures recorded at 2-cm intervals. With the catheters in their final locations, PWV was subsequently assessed in young and old rabbits during a graded intravenous infusion of phenylephrine (PE) at 2–10 $\mu g \cdot kg^{-1} \cdot min^{-1}$. The carotid artery was tied, the femoral artery repaired, and animals were survived after the study. Data were analyzed off-line with proprietary software (NIHem; Cardiovascular Engineering, Norwood, MA). In brief, proximal and distal pressures were signal averaged using the electrocardiographic (ECG) R-wave as a fiducial point. The foot-to-foot transit time was ascertained from signal-averaged waveforms. Transit distance was derived from linear fitting of the pullback data as previously described (36).

In Vivo Hemodynamic Studies

Young (5–9 mo, $n = 6$) and old (4–6 yr, $n = 6$) female NZW rabbits were sedated with ketamine/xylazine (25 $mg \cdot kg^{-1} \cdot 3.75$ $mg^{-1} \cdot kg^{-1}$ im), intubated, and ventilated with supplemental oxygen (2–4%). During the procedure, the rabbits were anesthetized with continuous intravenous infusion of ketamine and xylazine (5 and 4.5 $mg \cdot kg^{-1} \cdot h^{-1}$) as described (60). With the use of the right carotid artery, a 3-Fr dual pressure-volume catheter (Millar Instruments) was inserted through a 3-Fr sheath via the right carotid artery and advanced into the left ventricle (LV) under fluoroscopic guidance. With the use of four to five segments, the electrical impedance was measured within the LV, and data were recorded with LabChart7 Software (ADInstruments, Sidney, Australia) and MPVS Ultra Control Software (Millar Instruments) as high-fidelity, instantaneous LV pressure-volume loops during steady-state inferior vena cava (IVC) occlusion and saline calibration. To reduce preload to acquire systolic and diastolic pressure-volume relations, the IVC was occluded by physically compressing the IVC by applying pressure in the subxiphoid right lateral region of the abdomen. To obtain absolute volumes, blood resistivity was measured using ~1 ml of heparinized blood and a Rho cuvette, and parallel conductance was determined by the hypertonic saline method (42). The saline calibration was confirmed with echocardiography. Data were analyzed off-line with PVAN Ultra software (Millar).

Echocardiographic Studies

Transthoracic echocardiography was performed in sedated young (5–9 mo, $n = 5$) and old (4–6 yr, $n = 5$) female New Zealand White (NZW) rabbits (ketamine/xylazine 25 $mg \cdot kg^{-1} \cdot 3.75$ $mg^{-1} \cdot kg^{-1}$ im). A 7.5-mHz probe and long-axis and M-mode views were used. Analysis included LV and septal wall thickness, LV lumen diameter during systole and diastole, and LV fractional shortening and ejection fraction. Analyses were performed by an experienced echocardiographer blinded to the age.

In Vivo Electrophysiological Studies

Young (aged 5–7 mo, $n = 6$) and old (aged 3.5–5.5 yr, $n = 8$) female NZW rabbits were subjected to transvenous electrophysiological studies (EPS) as described (41). Briefly, rabbits were anesthetized with ketamine/xylazine (25 $mg \cdot kg^{-1} \cdot 3.75$ $mg^{-1} \cdot kg^{-1}$ im) and buprenorphine (0.03 mg/kg sq), intubated, and ventilated with isoflurane (1–2%, FI_{O_2} 0.5). Steerable 4-Fr decapolar and 4-Fr quadripolar EP catheters (Irvine Biomedical, Irvine, CA) were inserted in the right femoral and right jugular veins through 4-Fr sheaths and placed in the right atrium and ventricle, guided by fluoroscopy and pacing thresholds. Signals from the His bundle were obtained with the ventricular EP catheter [right ventricular (RV) base]. During the procedure, 12-lead surface, two intra-atrial, and five intraventricular ECG signals were recorded continuously using the EP-Bard-System Software OS2/warp (kindly provided by Bard, Lowell, MA), filtered with a bandwidth of 30–250 Hz (intracardiac signals) and 0.01–100 Hz (surface ECG). EPS were performed at a stimulation cycle length (CL) of 200 and 240 ms. The following electrophysiological parameters were analyzed as previously described (41): sinus node recovery time (SNRT) was evaluated at pacing drive rates of 200 and 240 ms after 200 beats, and the heart rate-corrected SNRT (SNRT − sinus CL) was calculated. Atrium-to-His (AH) and His-to-ventricle (HV) intervals that reflect conduction from the atrium to the proximal His bundle (AH) and from the His bundle via Purkinje fibers to the ventricle (HV) were measured. Antegrade and retrograde Wenckebach CL (AVWCL/VAWCL) were characterized as the longest CL resulting in Wenckebach atrioventricular (AV) block. Atrial effective refractory period, AV-nodal/His-Purkinje effective refractory period, and ventricular effective refractory periods in RV apex (VERPapex) and septal RV base (VERPbase) position were analyzed by progressively shortening the S2-interval in 10-ms steps after eight-beat S1 trains. To evaluate potential aging effects on QT duration, we applied the following previously established heart rate correction formulas for the expected QT interval under isoflurane anesthesia (10): WT, QT expected = $0.4 \times RR + 92$. The QT index was defined as the percentage of the observed vs. the expected QT. EPS were performed at baseline and during isoproterenol infusion (0.10–0.25 μg/min to increase the spontaneous heart rate to 120%).

Ex Vivo Optical Mapping

To further characterize electrophysiological changes in aging, we performed optical mapping studies of young (age 6–9 mo, $n = 6$–7) and old (age 3.5–6 yr, $n = 8$–9) female rabbits. Heart preparation and retrograde perfusion were performed as previously described (12). Briefly, hearts were stained with a voltage-sensitive dye, di-4 ANEPPS (Invitrogen, Carlsbad, CA). Blebbistatin (5 μM) was added to the perfusate to reduce motion artifacts (15). Fluorescence signals were recorded using a CMOS camera (100 × 100 pixels, 1,000 frames/s, 25 × 25-mm^2 field of view).

To measure and characterize anisotropic propagation, the center of the LV epicardium was stimulated with a concentric bipolar electrode (Harvard Apparatus) at 350 ms CL to generate an elliptical activation pattern from the stimulus site. Activation time point at each site was determined from the local action potential upstroke using $(dF/dt)_{max}$ and mapped using a custom-designed software based on Interactive Data Language (IDL 6.3; Research Systems), as previously described (12). Longitudinal and transverse conduction velocities were calculated by determining the major axis of conduction and estimating conduction along the direction of eigen vectors as previously described (12).

The spatial organization of wave propagations in VF was analyzed using cross correlation and correlation length analysis as described (12). Briefly, the reference channel was selected at the center of the LV free wall and correlation between reference, and the rest of the pixels were calculated and mapped. Higher correlation along the fiber orientation indicates activation during VF has preferential conduction along the fibers, as previously described (12). The correlation lengths along the longitudinal and the transverse direction were calculated, and the ratio of longitudinal/transverse was used for statistical test.

Sirius Red Staining

Rabbit hearts were excised ($n = 3$ young, $n = 3$ old female rabbits), fixed with 10% formalin, and embedded in paraffin. The hearts were cut in four-chamber view orientation at 5 μm thickness, deparaffinized, and stained with picro-Sirius red for 1 h at room temperature. After washes, sections on the slides were dehydrated in 100% ethanol and xylene and mounted in SHUR/Mount toluene-based liquid media (Triangle Biomedical Sciences, Durham, NC).

Analysis of Fibrosis

Sections stained with Sirius red were visualized with an Eclipse TE2000 microscope (Nikon, Melville, NY) and a ×4 objective under

white and polarized light, and the images were captured using Elements software (Nikon). The total and fibrotic areas were evaluated by capturing digital RGB images of the LV and septum wall. Analysis was performed using Adobe Photoshop software (Adobe Systems, San Jose, CA) and ImageJ software with the Otsu thresholding method (United States NIH, Bethesda, MD) as previously described and modified (1). The mean area of fibrosis was calculated by comparing total area (white light) and fibrotic area (polarized light) for young and old rabbit sections.

Magnetic Resonance Imaging

To assess structural correlates to age-related changes in the conduction system, hearts from young female (aged 6 mo, $n = 4$) and old (age 5 yr, $n = 3$) rabbits were excised and quickly fixed in 10% formalin solution. Two days before magnetic resonance imaging (MRI), fixed hearts were transferred to PBS solution to wash out residual fixative. Fluorocarbon solution (FC-43, Fluorinert; 3M, St. Paul, MN) was used to prevent dehydration and eliminate proton signal from the surrounding fluid (7).

The hearts were examined using a 17.6-T/89-mm vertical wide-bore magnet (Oxford Instruments, Oxford, UK) connected to a Bruker spectrometer console running Paravision 4 software (Bruker Instruments, Billerica, MA). The RF coil used for the in vitro imaging was a commercial birdcage coil (Bruker Instruments) with diameter = 25 mm and length = 35 cm. The temperature in the magnet was maintained at 19–20°C. Three-dimensional high-resolution MRI data were collected using a fast gradient echo pulse sequence, achieving a voxel resolution of 35 μm × 35 μm × 82 μm. Imaging parameters were TR = 150 ms, TE = 18.5 ms, 1 average, sampling bandwidth = 20 k. Total acquisition time was 7 h and 30 min. The subsequent high angular resolution diffusion microscopy (HARDM) using 21 directions was performed using a standard multislice PGSE pulse sequence, achieving an in-plane resolution of 60 μm × 60 μm with a slice thickness of 600 μm. The diffusion-sensitizing factor (b-value) was 1,000 s/mm^2 using $\Delta = 13.4$ ms and $\delta = 1.8$ ms. Imaging parameters were TR = 3,000 ms, TE = 25.1 ms, 1 average. Total acquisition scan time for each HARDM experiment was 7 h and 40 min. The pilot images with three orthogonal planes were collected at intervals during the experiment to determine if the isolated heart imbedded in the dense FC-43 solution moved during these long scans.

Data analysis. Volume rendering of the three-dimensional MR data sets was performed using ImageJ (version 1.41, http://rsbweb.nih.gov/ij/) that enabled appropriate virtual sectioning in any direction and geometrical image registration with the HARDM data sets. The tensor processing of HARDM data sets was performed using fanDTasia (2008, Barmpoutis, http://www.cise.ufl.edu/~abarmpou/) (3).

Explanation of the HARDM imaging interpretation. A diffusion tensor can be visualized as the intersection of two orthogonal ellipses, with the largest ellipse representing the preferential (or least restricted) direction of diffusion. The ellipse that is orthogonal to the largest ellipse is described by two additional vectors, which reflect diffusion barriers in this plane. If diffusion is isotropic (without barriers to diffusion), all three vectors that describe the ellipses are equal, and the volume that reflects the probability of water diffusion is represented by a sphere. If diffusion is restricted in one or more directions, it is referred to as anisotropic, and there are differences between the magnitudes of the three vectors. The term "eigen" is used to indicate that the calculated value is characteristic of the diffusion; eigen vector is defined as the orientation of diffusion, and eigen value reflects the rate of water diffusion. The orientation that is preferential, or least restricted, is known as the principal eigen vector. The rate of diffusion that corresponds to the principal eigenvector is known as the principal eigen value. The assignment of secondary and tertiary eigen vectors is dependent upon the magnitude of the corresponding eigen values and is made according to decreasing magnitude. Therefore, the principal, secondary, and tertiary eigen values are ordered in decreas-

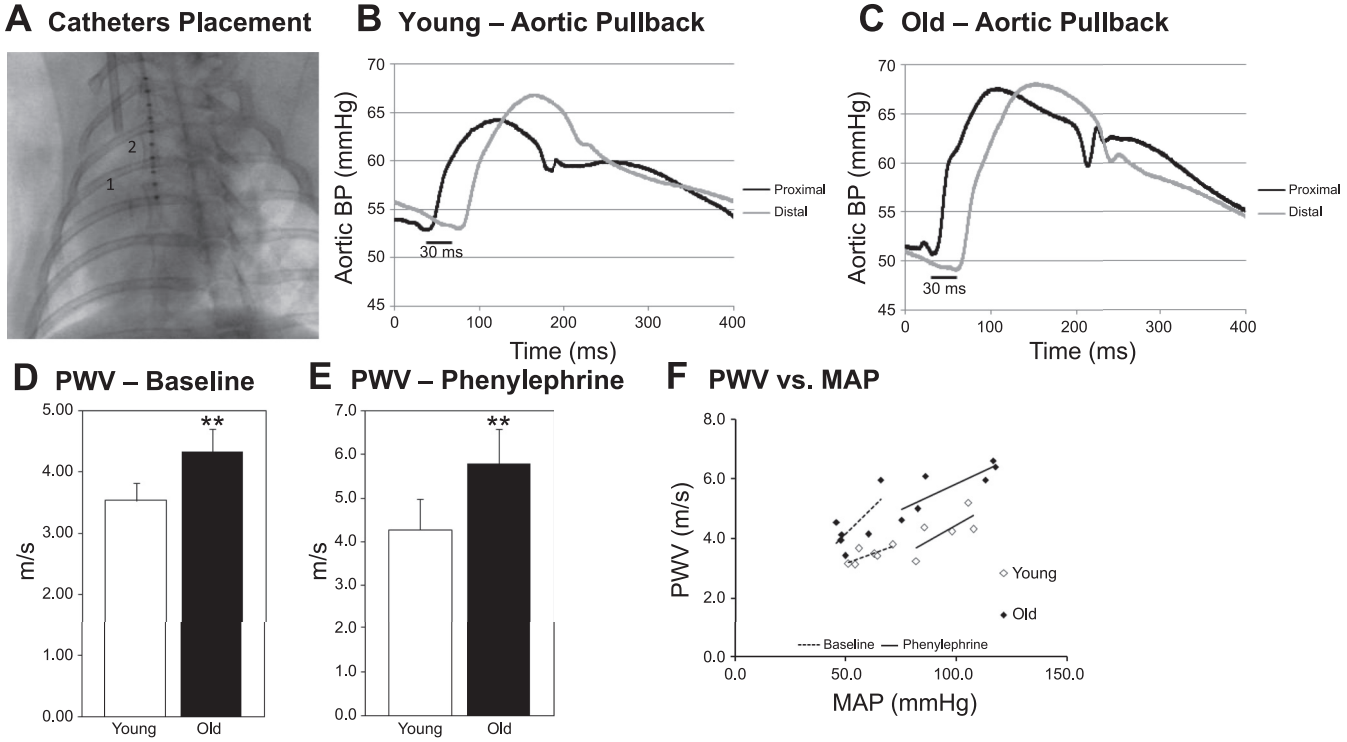

Fig. 1. Aortic pulse wave velocity (PWV) in young and old rabbits. *A*: fluoroscopic image of the placement of the two catheters. *B* and *C*: representative pressure tracings from young and old hearts at the end of the aorta during pullback procedure (proximal at 0 cm; distal at 10 cm). *D* and *E*: PWV at baseline ($n = 6$ young and $n = 6$ old rabbits) and with phenylephrine ($n = 5$ young and $n = 6$ old rabbits), respectively. $^{**}P < 0.01$. All values are shown as means ± SD. *F*: PWV vs. mean arterial pressure (MAP) of old and young rabbits at baseline and with phenylephrine. Data points represent individual rabbits of each group.

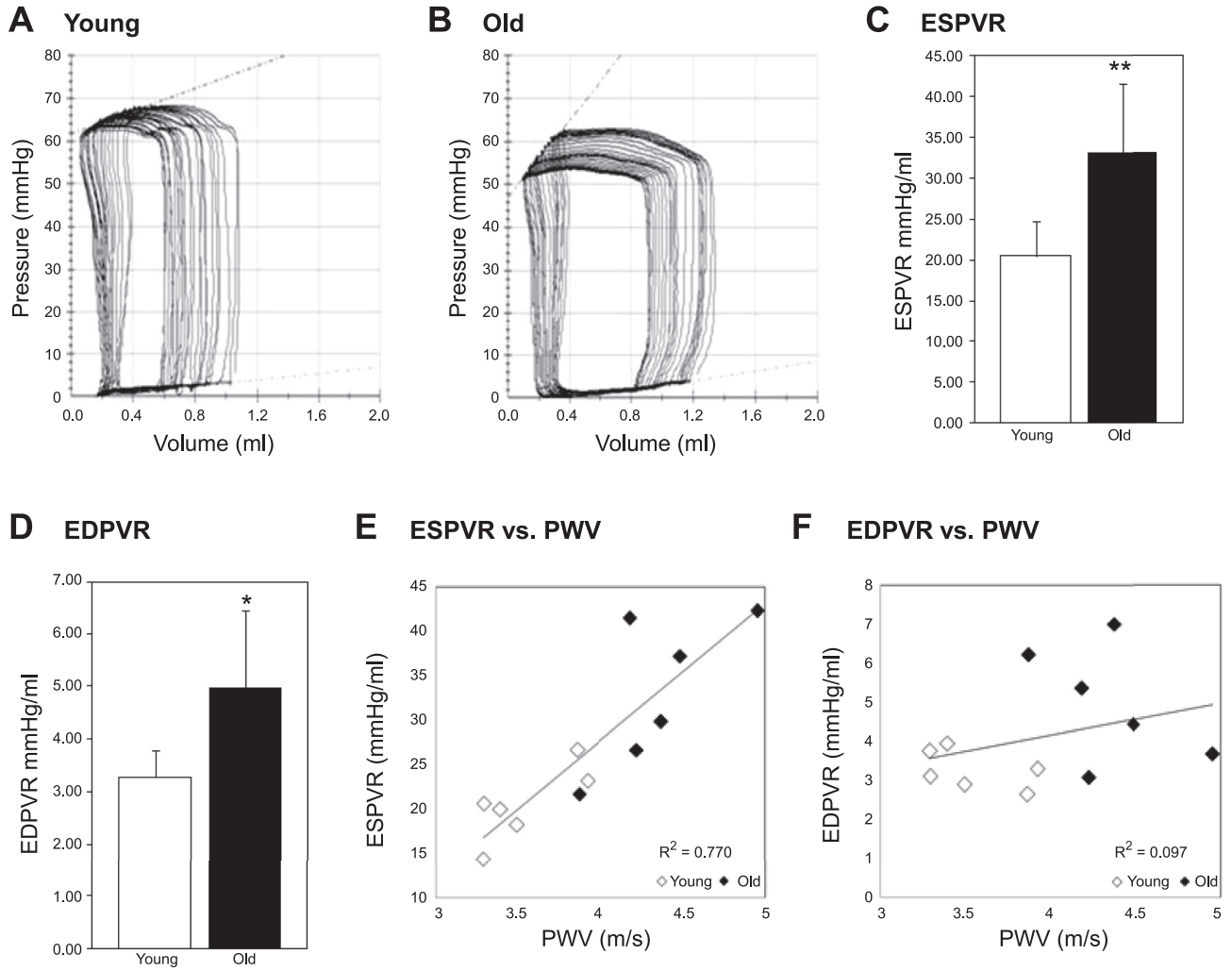

Fig. 2. Left ventricle (LV) hemodynamic parameters and relation to PWV in young and old rabbits. *A* and *B*: representative pressure-volume (PV) loops of individual young and old rabbits during occlusion of the inferior vena cava. *C*: end systolic pressure-volume relationship (ESPRV) in 6 young and 6 old rabbits. $^{**}P < 0.01$. *D*: end diastolic pressure-volume relationship (EDPVR) in 6 young and 6 old rabbits. $^{*}P < 0.05$. *E*: ESPVR vs. PWV in 6 young and 6 old rabbits, linear relationship: $y = 15.28x - 33.40$, $R^2 = 0.770$. *F*: EDPVR vs. PWV in 6 young and 6 old rabbits, no correlation: $y = 0.819x + 0.889$, $R^2 = 0.097$. All values are shown as means ± SD.

ing magnitude, and the corresponding eigen vectors reflect their direction. Previous work investigating diffusion in the heart suggests that the primary eigen vector reflects the orientation of the cardiomyofibers (19) and that the myocardial sheet structure proposed by LeGrice et al. (28) may be reflected by the tertiary eigen vector (19). A 3 × 3 diffusion tensor matrix, describing the three-dimensional translational diffusion of water molecules in each voxel, was calculated from the HARDM data set, and the three (primary, secondary, and tertiary) eigen vectors and eigen values were obtained (4, 5).

Statistical Analysis

For normally distributed values, we used Student's unpaired and paired *t*-tests to compare the means of two groups. Analysis was performed with Prism 4 for Windows (Graphpad, San Diego, CA). All data are presented as means.

RESULTS

In Vivo Hemodynamics and PWV

We first investigated PWV as an indicator of aortic stiffness. Figure 1*A* depicts the initial placement of the two catheters used during aortic pullback. Figure 1, *B* and *C*, shows old and young representative pressure tracings from the proximal pressure catheter in the aortic root and the distal femoral catheter at the femoral catheter's most distal point (10 cm). Baseline PWV

Table 1. *Echocardiographic data*

	IVS, mm	PW, mm	LVD, mm	LVS, mm	FS, %	EF, %
Young ($n = 5$)	2.66 (±0.39)	2.77 (±0.44)	13.51 (±2.02)	9.37 (±2.18)	30.86 (±10.29)	65.25 (±13.60)
Old ($n = 5$)	3.47 (±0.66)*	3.36 (±0.58)	13.50 (±2.58)	7.37 (±2.51)	29.41 (±6.30)	64.16 (±8.97)

Echocardiography of young and old rabbits. Values are means ± SD; *n*, no. of rabbits. EF, ejection fraction; FS, fractional shortening; IVS, intraventricular septum thickness; LVD, diastolic diameter of the left ventricle; LVS, systolic diameter of the left ventricle; PW, posterior wall thickness. Comparison of the IVS thickness, $^{*}P < 0.05$; All other comparisons, P = not significant.

and PWV under PE were significantly higher in old rabbits compared with young rabbits (baseline: young, 3.54 ± 0.36 vs. old, 4.35 ± 0.28 m/s, $P < 0.002$ and PE: 4.3 ± 0.8 vs. 5.8 ± 0.7 m/s, $P < 0.01$) (Fig. 1, *D* and *E*), indicating that stiffening of the aorta occurs with aging. Figure 1*F* depicts the relation between PWV and mean arterial pressure (MAP) in essentially nonoverlapping groups of young and old rabbits at baseline and during PE. Old rabbits tended to have lower MAP at baseline (young, 60.2 ± 7.5 vs. old, 53.2 ± 8.1, $P = 0.152$), whereas MAP was similar under PE infusion (young, 95.8 ± 11.6 vs. old, 98.7 ± 19.3, not significant). PE slowed heart rates in both young and old animals: young, baseline, 115 ± 20 vs. PE, 75 ± 13, paired *t*-test, $P < 0.001$ and old, 125 ± 13 vs. 85 ± 22, paired *t*-test, $P < 0.01$.

Second, we investigated the aging effect on LV stiffness. During IVC occlusion, the slopes of the end systolic pressure-volume relations (ESPRV) and end diastolic pressure-volume relations (EDPVR) were significantly altered in old compared with young rabbit hearts, as shown in Fig. 2, *A* and *B*. ESPRV was significantly higher in old rabbits (20.56 ± 4.2 vs. 33.14 ± 8.4 mmHg/ml, $P < 0.01$) (Fig. 2*C*), indicating an increased systolic stiffness and contractility in the aging heart. EDPRV was also significantly higher in old rabbits (3.28 ± 0.5 vs. 4.95 ± 1.5 mmHg/ml, $P < 0.05$) (Fig. 2*D*), indicating an increased diastolic stiffness and hence reduced compliance of the aging rabbit heart. Additionally, we observed a proportional, linear relation between PWV and ESPVR (Fig. 2*E*), indicating a parallel stiffening and remodeling of the aging heart and aorta. In contrast, no correlation was observed between PWV and EDPVR.

Echocardiographic Studies

Echocardiography data showed a 30% increase in wall thickness of the interventricular septum of old rabbits as well as a trend toward a thicker posterior wall, consistent with concentric hypertrophy (Table 1). Moreover, old rabbits had an increased LV mass (young, $n = 7$, 8.26 ± 0.55 vs. old, $n = 5$, 12.11 ± 1.48, $P < 0.05$), but the LV mass-to-body weight ratio was not changed with aging. No differences were observed between old and young rabbits in regard to ejection fraction, fractional shortening, LV diastolic diameter, and LV systolic diameter (Table 1).

In Vivo EPS

During in vivo EPS, the heart rate was significantly slower in old rabbits (young vs. old, 184 ± 4 vs. 166 ± 6 beats/min, $P < 0.05$) at baseline and slower during isoproterenol exposure (212 ± 17 vs. 200 ± 11 beats/min, $P < 0.05$), but isoproterenol significantly increased heart rate in both young and old rabbits ($P < 0.05$ each, paired *t*-test). In line with the slower heart rate in old rabbits, in vivo EPS revealed a longer heart rate-corrected SNRT in old rabbits at baseline (78.4 ± 23.4 vs. 126.0 ± 24.1 ms, $P < 0.05$) and after sympathetic stimulation (70.0 ± 13.6 vs. 109.0 ± 29.5 ms, $P < 0.05$ each).

Figure 3, *A* and *B*, depicts representative alterations in QRS morphology and duration in old rabbits, demonstrating classical right bundle branch block (RBBB) features with an rR′ QRS morphology in V1 and a broad S in V5, V6 along with the typically seen inverted T-wave in V1. We observed this classical complete RBBB morphology in four out of eight old

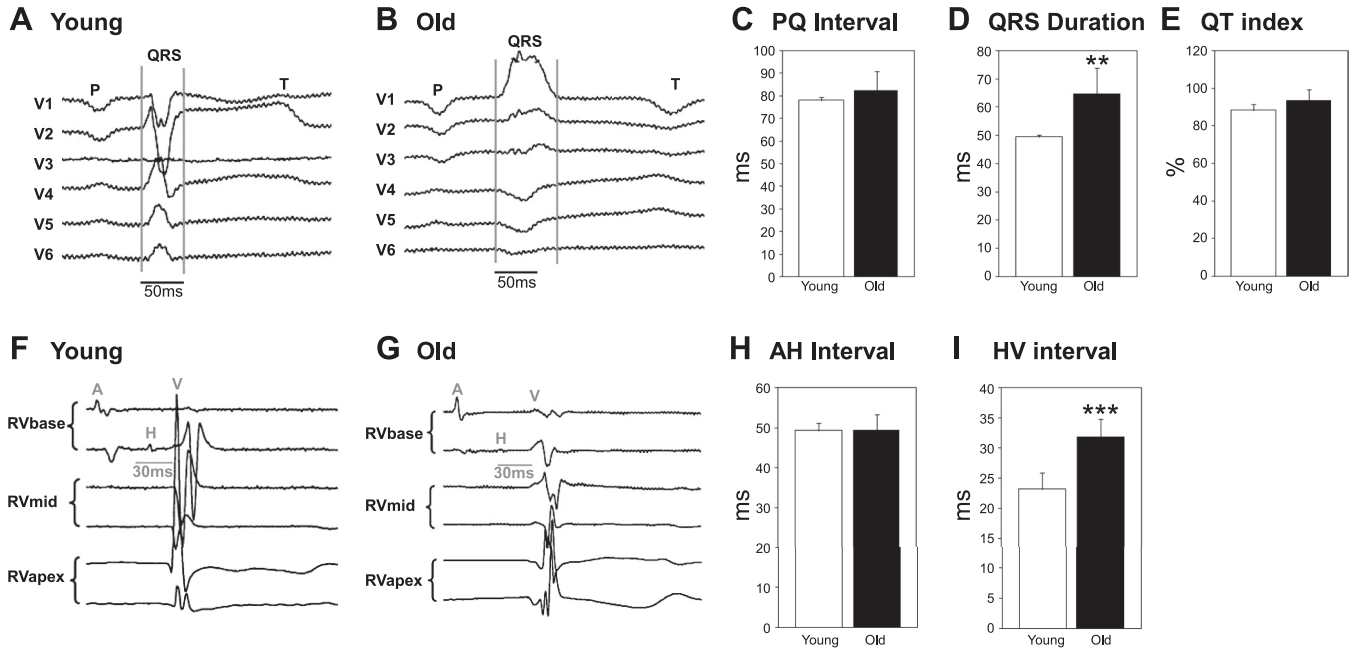

Fig. 3. Electrocardiographic (ECG) parameters in young and old rabbits. *A* and *B*: representative ECG traces (chest leads V1–V6) of individual young and old rabbits, demonstrating classical right bundle branch block (RBBB) features along with the typically seen inverted T-wave in V1. P, P wave, QRS complex; T, T wave. *C*: PQ interval duration in 6 young and 8 old rabbits. *D*: QRS duration in 6 young and 8 old rabbits. $^{**}P < 0.01$. *E*: heart rate-corrected QT index (QT_i) in 6 young and 8 old rabbits. All values are shown as means ± SD. *F* and *G*: representative intracardiac ECG traces (RV apex, mid, and base position) of individual young and old rabbits. A, atrium; H, His electrogram; V, ventricle. *H*: duration of AH intervals, which reflect conduction from the atrium to the proximal His bundle, in 6 young and 8 old rabbits. *I*: duration of HV intervals, which reflects conduction from the His bundle via Purkinje fibers to the ventricle, in 6 young and 8 old rabbits. $^{***}P < 0.0001$. All values are shown as means ± SD.

rabbits; the other four old rabbits had incomplete RBBB-like QRS patterns. In contrast, all young rabbits had normal QRS patterns in leads V1–V6 as shown in Fig. 3*A*. These age-related changes in QRS resulted in significantly prolonged QRS complex durations in old rabbits ($P < 0.01$, Fig. 3*D*). Moreover, we observed a trend toward longer PQ intervals in old rabbits (78.0 ± 1.6 vs. 82.4 ± 8.7 ms, $P = 0.295$, Fig. 3*C*). Heart rate-corrected QT indexes did not differ between old and young rabbits (Fig. 3*E*). In vivo EPS revealed prolonged HV intervals in old rabbits (HV: 23 ± 2.5 vs. 31.9 ± 2.9 ms, $P < 0.0001$, Fig. 3, *F*, *G*, and *I*), indicating a slowed conduction, particularly through the His-Purkinje system in old rabbits. However, AH intervals (Fig. 3*H*), AV Wenckebach cycle length (AVWCL: 163.3 ± 15.1 vs. 165.7 ± 17.2 ms), and AV nodal effective refractory periods (10 ± 15.8 vs. 106.7 ± 13.7 ms) did not differ between both age groups, indicating a lack of age-related changes in the AV nodal conduction.

VERP in the RV apex and base did not differ between old and young rabbits (VERP240 apex, 140.0 ± 8.9 vs. 147.5 ± 14.9 ms; VERPbase: 150 ± 22.8 vs. 155 ± 16 ms). However, the isoproterenol-induced shortening of the VERP was more pronounced in young rabbits where a significant shortening occurred in both the apex and the base (VERP240apex-Iso, young, 128.3 ± 14.7 ms, $P < 0.05$ vs. baseline; VERP240base-Iso, 136.7 ± 13.7 ms, $P < 0.05$ vs. baseline) while in old rabbits the VERP only shortened in the base (VERP240apex-Iso, old, 141.3 ± 17.3 ms; VERP240base-Iso, 137.1 ± 12.8 ms, $P < 0.05$ vs. baseline).

Tissue Anisotropy and VF Inducibility

We further investigated CV changes and VF inducibility of young and old hearts using optical mapping. Activation maps under sinus rhythm show marked delay in old heart (Fig. 4, *A–C*) and the total activation time from the field of view was longer in line with the widening of the QRS complex in old hearts (see Fig. 3). However, action potential duration (APD) (young, 210.39 ± 15.55 vs. old, 206.18 ± 19.57) and APD dispersion did not differ between young and old hearts (Fig. 4, *D–F*). Figure 4, *G* and *H*, shows typical examples of elliptical activation patterns during LV stimulation. In the aging heart, the anisotropic conduction became more exaggerated: in the old heart, longitudinal conduction velocity (CV_L) = 0.828 ± 0.053 ms/transverse conduction velocity (CV_T) = 0.280 ± 0.078 ms, whereas, in the young heart, CV_L = 0.767 ± 0.091

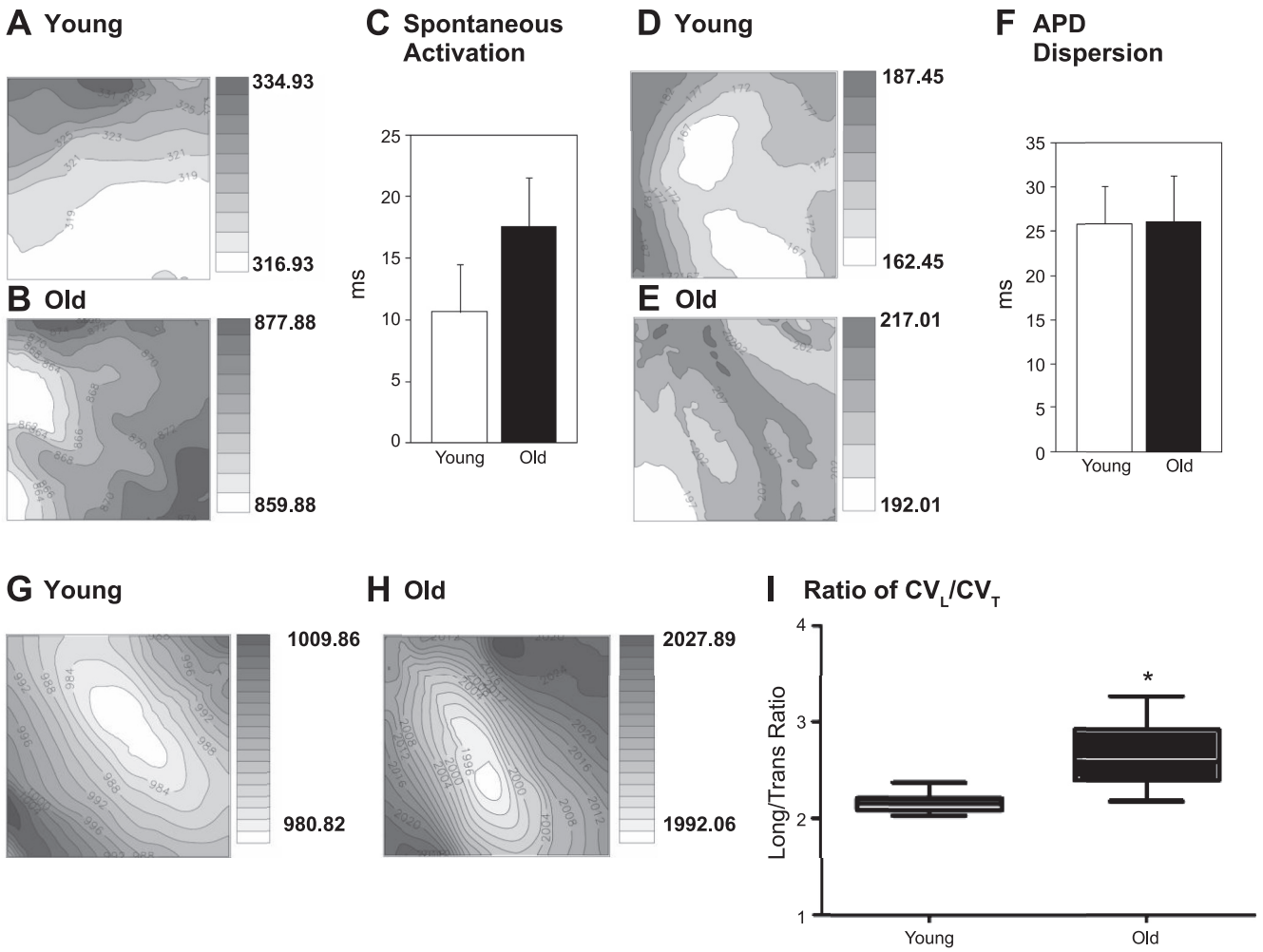

Fig. 4. Optical mapping in young and old hearts. *A–C*: representative maps and graph of spontaneous activation from the LV in 6 young and 9 old hearts. Isochronal lines are drawn in 2-ms intervals, and brighter color indicates earlier activation. P = not significant (NS). *D–F*: representative action potential dispersion maps and graph in 6 young and 8 old hearts. P = NS. *G* and *H*: representative activation maps and graph from LV center stimulation. *I*: ratio of longitudinal conduction velocity (CV_L) to transverse conduction velocity (CV_T) in 7 young and 9 old hearts.*$P < 0.05$; all values are shown as means ± SD.

ms/CV_T = 0.348 ± 0.047 ms. Figure 4*I* shows box plots of the distribution of longitudinal and transverse CV (CV_L/CV_T), with an increase of the CV_L-to-CV_T ratio and a greater variation mostly in old hearts ($P < 0.05$), suggesting that conduction in the transverse direction is hindered with age compared with the longitudinal direction.

We further investigated whether changes in tissue anisotropy in aging can cause different wave dynamics in VF. VF was inducible in most old hearts (7 out of 9) and only a few young hearts (3 of 12) by the ramp pacing protocol (systematic decrease in stimulation CL). Typical examples of VF signals from young and old hearts are shown in Fig. 5, *A* and *B*. Because transverse conduction is hampered in aging hearts, we hypothesized that conduction blocks across the transverse direction may provide a substrate for VF maintenance. The superimposed traces along the transverse direction in old hearts (Fig. 5, *C* and *D*, panels on *bottom*) also show asynchronous membrane potential (V_m) oscillations, indicating anomalies in transverse conduction in old hearts may contribute to VF maintenance. To quantify abnormal conduction in the transverse direction in VF, we applied cross correlation analysis (with correlation of V_m oscillations between different pixels in VF). The center of field of view was selected as reference, and correlation between the rest of the field of view was calculated and mapped in Fig. 5, *C* and *D* (panels on *top*). In line with CV_L/CV_T measurements, old hearts show lower correlation along the transverse direction, resulting in more elongated elliptical correlation maps.

Fibrosis in the Aging Heart

Histochemical experiments revealed an age-related increase of total (5.60 ± 0.1 vs. 11.01 ± 0 1.3%, $P < 0.01$) and interstitial (defined as total fibrosis − fibrosis around the epicardium, valves, and large vessels) (2.82 ± 0.5 vs. 6.97 ± 0.8%, $P < 0.01$) fibrosis in the LV and interventricular septum (Fig. 6).

Structural Changes in the Aging Heart

In line with the increased wall thickness of the interventricular septum assessed in vivo by echocardiography, we observed a significant increase in interventricular septum thickness in the young ($n = 4$) and old ($n = 3$) rabbit hearts using MRI (3.87 ± 0.08 vs. 4.81 ± 0.60 mm, $P < 0.05$). Moreover, volume-rendered transverse images of the apical half of the LV suggest that the free-running Purkinje fiber network in the LV cavity is significantly altered with aging (Fig. 7, *A* and *B*). Young hearts have a higher complexity in the geometry of free-running fibers than hearts from older animals. In addition, young hearts have free-running fibers that are significantly larger in diameter (0.2 ± 0.01 vs. 0.14 ± 0.018 mm, $P < 0.05$).

Results of HARDM are presented in Fig. 7, *C* and *D*, which shows typical, representative tensor component maps of hearts from a young and an old rabbit. The heart from the young animal shows a conspicuous stripe pattern in the interseptum and free wall (Fig. 7*C*). This pattern is less apparent in the heart from the older animal (Fig. 7*D*). A volume-rendered image of the interventricular septum shows that the stripe pattern has a

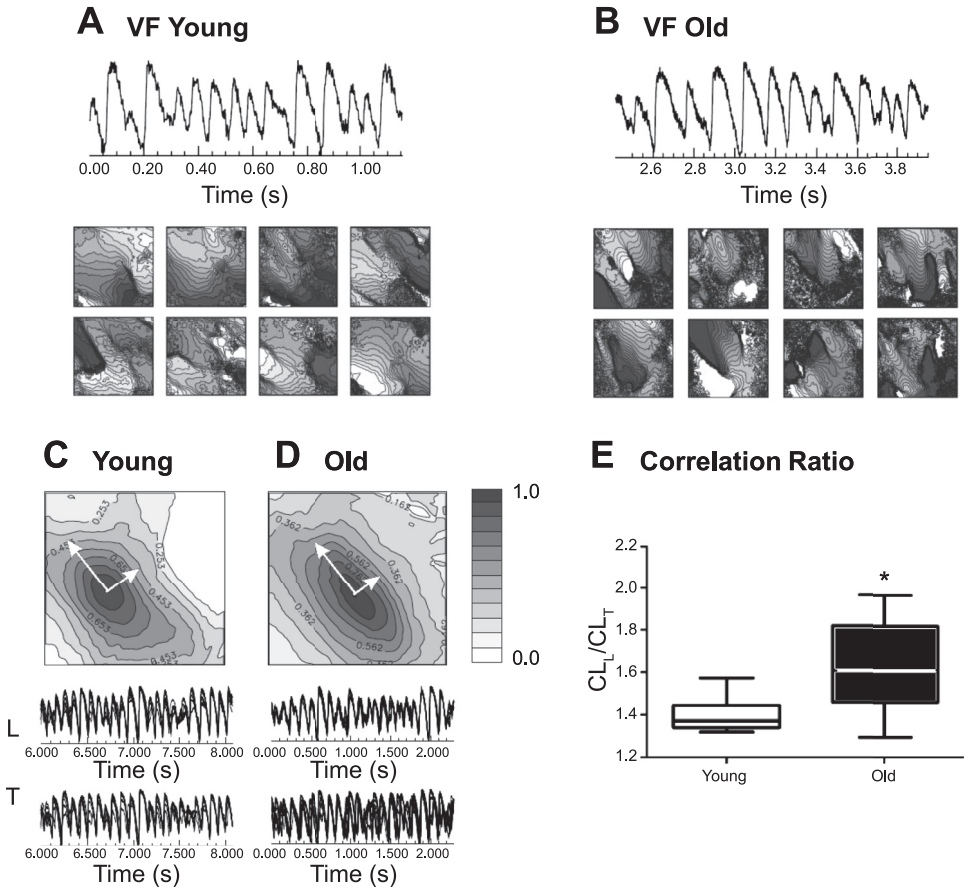

Fig. 5. Ventricular fibrillation (VF) in young and old hearts. *A* and *B*: representative series of activation maps of hearts during VF from the LV in 3 young and 7 old hearts. Isochronal lines are drawn at 2-ms intervals, and brighter colors indicate earlier activation. *C* and *D*: cross-correlation of propagating waves in the longitudinal (L) and transverse (T) directions of individual young and old rabbit hearts during VF. *E*: box graphs of correlation length ratio (CL_L/CL_T) in 3 young and 7 old rabbit hearts. *$P < 0.05$; all values are shown as means ± SD.

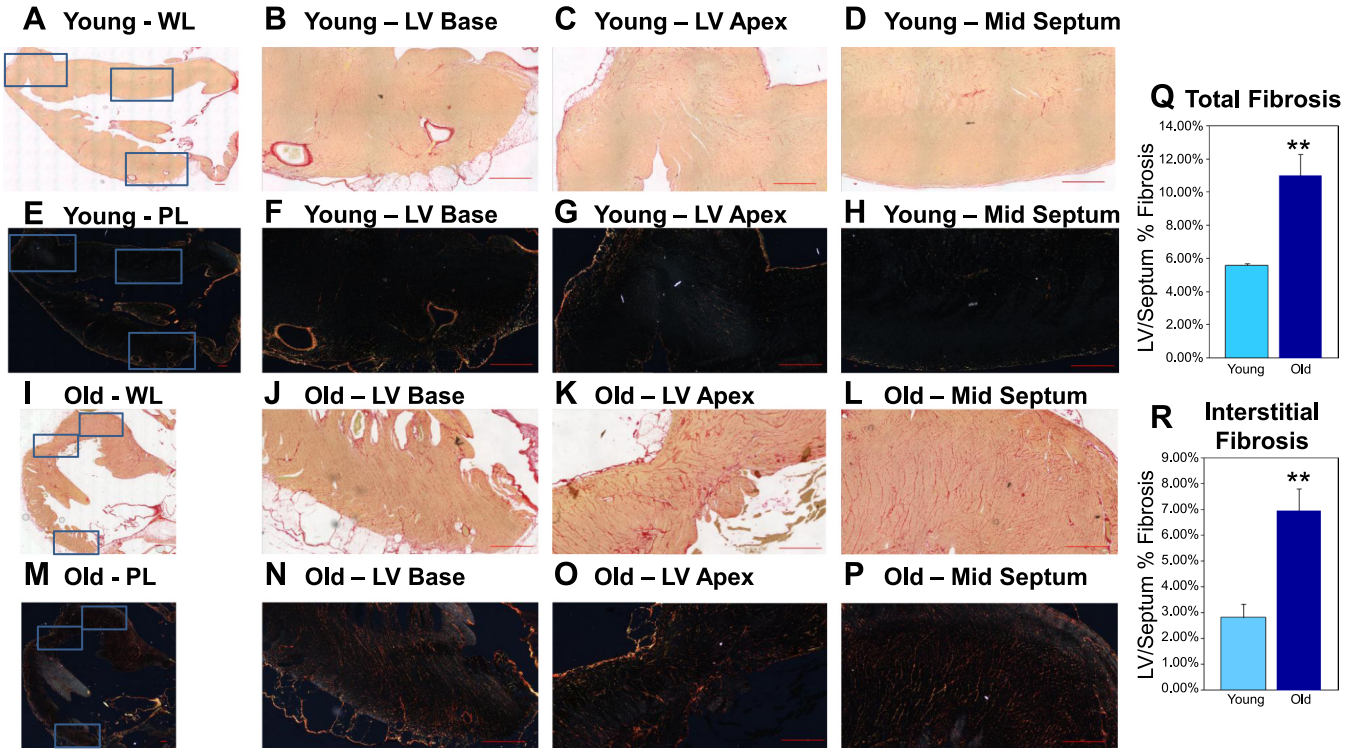

Fig. 6. Fibrosis analysis in young and old hearts. *A–P*: representative Sirius red stainings of the LV and septum of young hearts under white and polarized light. *Q* and *R*: total and interstitial fibrosis as a percentage of the LV and the septum in young ($n = 3$) and old ($n = 3$) rabbit hearts. $^{**}P < 0.01$; all scale bars = 1,000 μm. All values are shown as means ± SD.

longitudinal direction and appears to exist in the basal half of the LV. Figure 7, *E* and *F*, compares the primary eigen vector and the tertiary eigen vector in the midinterventricular septum of a young heart and an old heart. These correspond to the myocardial fiber orientation and the orientation of the myocardial sheet structure, respectively (20, 51). These transmural patterns are less distinct in the old heart, and the orientation of the tertiary eigen vectors is dramatically altered as well.

DISCUSSION

In this study, we reveal age-related functional, electrical, and morphological changes in the heart and the aorta, such as an increased aortic stiffness that is associated with decreased diastolic and systolic compliance, increased fibrosis and altered myofibrillar orientation and myocardial sheet structure in the septum, slowed CV and increased CV anisotropy in the ventricle and the His-Purkinje conduction system, and Purkinje fiber network deterioration. Thus, this study provides a detailed assessment of various components of ventricular and vascular aging that may contribute to heightened arrhythmogenic risk with advancing age.

Aging and Structural and Functional Changes in the Heart and Aorta

We show age-related alterations in diastolic and systolic mechanical function as previously shown in humans (32, 43). The end-diastolic elastance is increased in old rabbits, indicating a decreased diastolic compliance as previously described in older humans with a reduced LV filling rate (6, 26, 50) and an age-related increase in operant end-diastolic elastance (8). Moreover, we observed an age-related increase in end-systolic elastance, indicating that myocardial stiffness and contractility are also increased during systole. We hypothesize that changes in ventricular stiffness associated with cardiac remodeling are coupled to arterial remodeling during the aging process. It is well known that arterial stiffness, wave reflections, and systolic and pulse pressures all increase with aging in humans (26, 35). We confirmed that, in the rabbit model, PWV and, hence, aortic stiffness also increase with aging. In humans <50 years of age, the PWV typically ranges from 5 to 7 m/s; whereas, in humans >60 years of age, PWV ranges from 8 to 11 m/s or higher (35, 44), which is considerably higher than PWV values observed during aortic pullback experiments in our rabbits. For these studies, however, baseline measures were acquired while the rabbits were anesthetized with ketamine and xylazine, which considerably lowered blood pressure. At baseline, old rabbits tend to have lower MAP yet higher PWV, and, under α_1-adrenergic stimulation, young and old rabbits have similar MAP while old rabbits have much higher PWV. Additionally, the relative difference in PWV between young and old was more comparable between humans and rabbits when evaluated at the higher pressures generated by α_1-adrenergic stimulation. Because it has been shown that higher resting heart rate and an acute increase in heart rate are associated with higher PWV, lower heart rate cannot explain higher PWV during PE infusion (2, 23, 27, 31, 35). Moreover, we were able to show a positive, linear relation between aortic stiffness and cardiac stiffness during systole, whereas no relation existed between aortic and diastolic cardiac stiffness, suggesting that aortic stiffness leads to systolic stiffening of the aging heart.

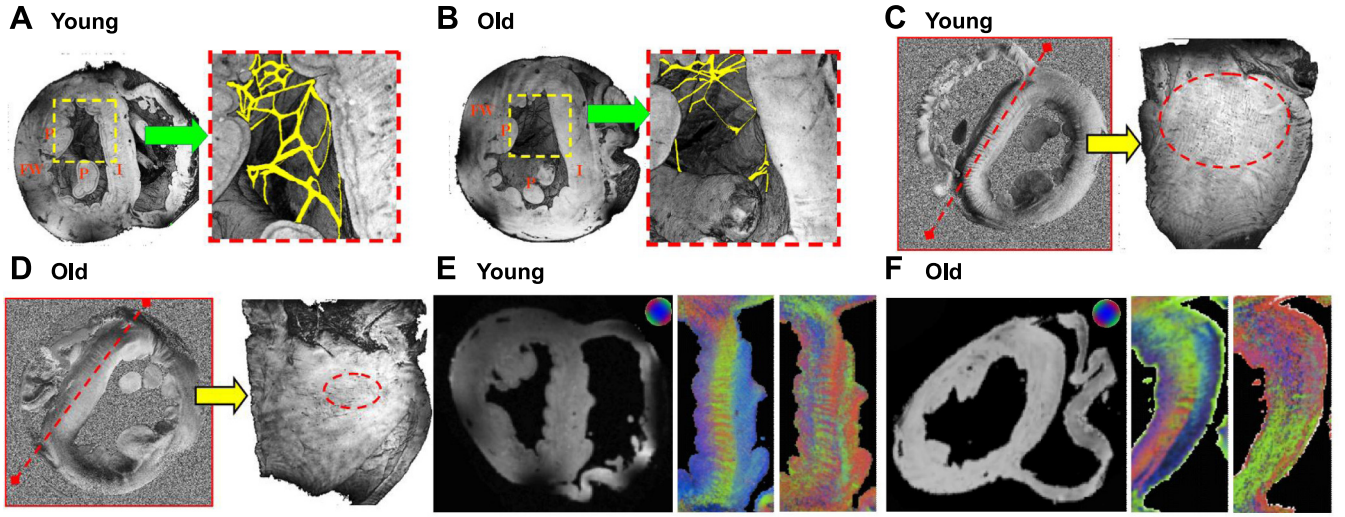

Fig. 7. Magnetic resonance imaging (MRI) parameters in the young and old heart. *A* and *B*: representative volume-rendered transverse images and manual segmentation (magnified) of the free-running Purkinje fiber network in the LV of an individual young and old rabbit heart. Lines and arrows in the green and red boxes indicate where virtual sectioning occurred in the long-axis planes. Interventricular septum thickness is ~3.93 mm (young) and 4.82 mm (old). I, interventricular septum; P, papillary muscle; FW, free wall. *C* and *D*: representative tensor component (D_{yz}) map from high angular resolution diffusion microscopy and a volume-rendered image of the interventricular septum of an individual young and old rabbit heart. Dotted lines (red) indicate where sectioning occurred, and dotted circles confine regions where the stripe pattern is observed. *E* and *F*: the primary eigen vector and the tertiary eigen vector maps of the left interventricular septum of young and old rabbit hearts. The primary eigen vector shows the preferential direction of water diffusion and is known to follow cardiomyofibers and conducting fiber tracts. Note the rotation of the color wheel orientation in *E* and *F*. The color wheel located at the top of each panel reflects the directional orientation of the respective eigen vectors. Blue represents eigen vectors that are through-plane (e.g., traveling out the page), whereas the colors red and green reflect in-plane orientations. Septal images have been rotated to allow comparison, and the color wheels have been rotated to the same extent to maintain the correct orientation for directionality.

In rabbits, aging increased LV wall thickness but did not alter systolic LV function as assessed by ejection fraction, which is similar to the pattern observed in aging humans in the absence of hypertension or cardiovascular disease (26). We observe a simultaneous increase in aortic and diastolic stiffness, increased systolic contractility and elastance, and maintenance of the ejection fraction with age, which reinforces this idea that ventricular performance is coupled with arterial function. Hence, when we correlate both systolic and diastolic indexes of ventricular function with aortic PWV, we observed that only systolic stiffness is strongly associated with progressive aortic stiffness with age, suggesting that an age-related concentric remodeling of the LV in response to stiffening of the aorta maintains ejection fraction in the presence of hypertrophy and diastolic dysfunction.

Aging and Electrophysiological and Structural Properties of the His-Purkinje System

We show aging-related impaired sinus node function and slowed AV conduction, similarly as in humans (16, 18, 48). However, while it has been demonstrated by various groups that aging prolongs PQ interval durations mainly by slowing of conduction through the AV node and proximal His bundle due to increased fibrosis in the specialized conduction system (16, 18, 48), we revealed a pronounced slowing of conduction, particularly through the distal His-Purkinje system resulting in prolonged HV intervals and broader QRS complexes. Similarly, in comprehensive EPS, prolonged HV intervals were described in older individuals (55). However, so far, the mechanisms underlying this impaired conduction through the distal His-Purkinje system remained unclear. Using high-resolution MRI, we revealed that alterations in His-Purkinje function were associated with morphological changes in the Purkinje system consisting of a thinned reticular network with fewer connections and thinner individual free-running Purkinje fibers. Whether age-related morphological changes in the human Purkinje system similar to those that we have described in the rabbit might underlie slowed conduction in humans remains to be investigated.

Tensor component maps of young hearts derived from HARDM data show a conspicuous stripe pattern in the interventricular septum and free wall that becomes less apparent in hearts from older animals. This stripe pattern has a longitudinal direction and appears to exist in the basal half of the LV. Considering that a basal end of these longitudinal stripes is proximal to the membranous interventricular septum from where the left bundle originates (9, 40), the stripe patterns visible by endogenous MR contrast could represent projections from the left bundle that form the fan-like structure in the subendocardium of the interventricular septum. Combined analysis of the two MR modalities (magnetic resonance microscopy and HARDM) may provide a powerful tool to understand and monitor alterations in myofibrillar orientation, myocardial sheet structure, and the cardiac conduction network that occur as a result of aging.

Aging and Structural and Electrophysiological Properties of the Ventricle

Similar to observations in aging humans, we show that ventricular stiffness and wall thickness increase in the aging rabbit heart. Myocardial sheet structure reorientation has been shown to contribute to myocardial wall thickening in rats (11). Here, we show that increased wall thickness and alterations of myofibrillar and myocardial sheet orientation are both positively associated with age. Whether these age-related changes in myofibrillar and

myocardial sheet orientation directly contribute to ventricular stiffness, however, remains to be investigated. Moreover, alterations in cell excitation and calcium handling also contribute to the age-related changes in the electrophysiological properties of the ventricle. It has been shown that cardiomyocytes from aging animals have longer action potentials primarily due to increased inward L-type current and reduced outward potassium currents (21, 58). Also, several studies in murine models have shown changes in calcium-handling proteins, such as sarco(endo)plasmic reticulum Ca^{2+}-ATPase (SERCA), phospholamban, L-type calcium channel, ryanodine receptor, and sodium/calcium exchanger (21, 29, 30, 49, 52, 59, 62). Also, functional changes in calcium handling, particularly with regard to SERCA, have been associated with both systolic and diastolic dysfunction (17, 49, 59). These alterations suggest that age-related cellular and molecular changes are plausible culprits behind the slowing of CV as well as triggered activity associated with the aging proarrhythmogenic phenotype.

Several reports have suggested that fibrosis in aging may increase the anisotropy of the ventricular muscle and may play an important role in the initiation and maintenance of VF through conduction blocks along the transverse direction (24, 39, 56, 63). Using epicardial optical mapping, we revealed an increase in anisotropic conduction. Increased conduction anisotropy was associated with a higher VF-inducibility rate and a changed spatial organization of wave propagations during VF in old rabbits, suggesting that increased CV anisotropy provided a proarrhythmogenic substrate. Similarly, age-related reductions in transverse CV have been described in rabbits (13), mice (54), and dogs (25) and were attributed to increased fibrosis and reduced intercellular coupling in old myocardium. Using HARDM, we have shown that not only increased fibrosis but also alterations of the myofibrillar orientation and myocardial sheet structure accompany age-related slowing of ventricular CV and increased conduction anisotropy. Moreover, these age-related changes in myocardial sheet and fiber orientation likely provide a structural substrate for reentrant arrhythmias, thereby increasing susceptibility to VF.

In summary, we have provided a detailed assessment of the impact of aging on the electromechanical structure and function of the rabbit heart. The rabbit model shows a parallel age-related increase in aortic and ventricular stiffness, as is seen in older humans. Moreover, aging slows CV throughout the His-Purkinje system and changes the morphology of the Purkinje network. The old rabbit heart also has an increased ventricular conduction anisotropy probably because of fibrosis and changed myofibrillar orientation and myocardial sheet structure, which provides a proarrhythmogenic substrate and thereby contributes to pathogenesis of VF in old hearts. Thus, the aging rabbit model represents a useful tool for elucidating age-related changes that predispose the aging heart to arrhythmia and sudden cardiac arrest.

ACKNOWLEDGMENTS

We thank Paul Jeng, Divyang Patel, and Ohad Ziv for support, assistance with data analysis, and preparation of figures.

DISCLOSURES

No conflicts of interest, financial or otherwise, are declared by the authors.

AUTHOR CONTRIBUTIONS

Author contributions: L.L.C., K.E.O., M.-S.H., G.F.M., J.R.F., B.-R.C., and G.K. conception and design of research; L.L.C., K.E.O., M.-S.H., L.C., L.S., C.A.T., and B.-R.C. performed experiments; L.L.C., K.E.O., M.-S.H., C.A.T., A.S.G., and B.-R.C. analyzed data; L.L.C., K.E.O., M.-S.H., C.A.T., G.F.M., J.R.F., B.-R.C., and G.K. interpreted results of experiments; L.L.C., K.E.O., M.-S.H., C.A.T., and B.-R.C. prepared figures; L.L.C., K.E.O., M.-S.H., and B.-R.C. drafted manuscript; L.L.C., K.E.O., M.-S.H, G.F.M., J.R.F., B.-R.C., and G.K. edited and revised manuscript; L.L.C., K.E.O., M.-S.H., L.C., L.S., C.A.T., A.S.G., G.F.M., J.R.F., B.-R.C., and G.K. approved final version of manuscript.

REFERENCES

1. **Andersen A, Nielsen JM, Peters CD, Schou UK, Sloth E, Nielsen-Kudsk JE.** Effects of phosphodiesterase-5 inhibition by sildenafil in the pressure overloaded right heart. *Eur J Heart Fail* 10: 1158–1165, 2008.
2. **Avolio A, Jones D, Tafazzoli-Shadpour M.** Quantification of alterations in structure and function of elastin in the arterial media. *Hypertension* 32: 170–175, 1998.
3. **Barmpoutis A, Vemuri B.** A unified framework for estimating diffusion tensors of any order with symmetric positive-definite constraints. In: *IEEE International Symposium on Biomedical Imaging* 2010, p. 1385–1388.
4. **Basser PJ.** Focal magnetic stimulation of an axon. *IEEE Trans Biomed Eng* 41: 601–606, 1994.
5. **Basser PJ, Mattiello J, LeBihan D.** MR diffusion tensor spectroscopy and imaging. *Biophys J* 66: 259–267, 1994.
6. **Benjamin EJ, Levy D, Anderson KM, Wolf PA, Plehn JF, Evans JC, Comai K, Fuller DL, Sutton MS.** Determinants of Doppler indexes of left-ventricular diastolic function in normal subjects (the Framingham Heart-Study). *Am J Cardiol* 70: 508–515, 1992.
7. **Benveniste H, Blackband S.** MR microscopy and high resolution small animal MRI: applications in neuroscience research. *Prog Neurobiol* 67: 393–420, 2002.
8. **Borlaug BA, Lam CSP, Roger VL, Rodeheffer RJ, Redfield MM.** Contractility and ventricular systolic stiffening in hypertensive heart disease insights into the pathogenesis of heart failure with preserved ejection fraction. *J Am Coll Cardiol* 54: 410–418, 2009.
9. **Bosch X, Theroux P, Roy D, Moise A, Waters DD.** Coronary angiographic significance of left anterior fascicular block during acute myocardial infarction. *J Am Coll Cardiol* 5: 9–15, 1985.
10. **Brunner M, Peng X, Liu GX, Ren XQ, Ziv O, Choi BR, Mathur R, Hajjiri M, Odening KE, Steinberg E, Folco EJ, Pringa E, Centracchio J, Macharzina RR, Donahay T, Schofield L, Rana N, Kirk M, Mitchell GF, Poppas A, Zehender M, Koren G.** Mechanisms of cardiac arrhythmias and sudden death in transgenic rabbits with long QT syndrome. *J Clin Invest* 118: 2246–2259, 2008.
11. **Chen JJ, Liu W, Zhang HY, Lacy L, Yang XX, Song SK, Wickline SA, Yu X.** Regional ventricular wall thickening reflects changes in cardiac fiber and sheet structure during contraction: quantification with diffusion tensor MRI. *Am J Physiol Heart Circ Physiol* 289: H1898–H1907, 2005.
12. **Choi BR, Liu T, Lavasani M, Salama G.** Fiber orientation and cell-cell coupling influence ventricular fibrillation dynamics. *J Cardiovasc Electrophysiol* 14: 851–860, 2003.
13. **Dhein S, Hammerath SB.** Aspects of the intercellular communication in aged hearts: effects of the gap junction uncoupler palmitoleic acid. *Naunyn Schmiedebergs Arch Pharmacol* 364: 397–408, 2001.
14. **Eghbali M, Robinson TF, Seifter S, Blumenfeld OO.** Collagen accumulation in heart ventricles as a function of growth and aging. *Cardiovasc Res* 23: 723–729, 1989.
15. **Fedorov VV, Lozinsky IT, Sosunov EA, Anyukhovsky EP, Rosen MR, Balke CW, Efimov IR.** Application of blebbistatin as an excitation-contraction uncoupler for electrophysiologic study of rat and rabbit hearts. *Heart Rhythm* 4: 619–626, 2007.
16. **Fleg JL, Das DN, Wright J, Lakatta EG.** Age-associated changes in the components of atrioventricular conduction in apparently healthy volunteers. *J Gerontol* 45: M95–M100, 1990.
17. **Froehlich JP, Lakatta EG, Beard E, Spurgeon HA, Weisfeldt ML, Gerstenblith G.** Studies of sarcoplasmic reticulum function and contraction duration in young adult and aged rat myocardium. *J Mol Cell Cardiol* 10: 427–438, 1978.
18. **Gottwald M, Gottwald E, Dhein S.** Age-related electrophysiological and histological changes in rabbit hearts: age-related changes in electrophysiology. *Int J Cardiol* 62: 97–106, 1997.
19. **Helm PA, Tseng HJ, Younes L, McVeigh ER, Winslow RL.** Ex vivo 3D diffusion tensor imaging and quantification of cardiac laminar structure. *Magn Reson Med* 54: 850–859, 2005.
20. **Hsu EW, Muzikant AL, Matulevicius SA, Penland RC, Henriquez CS.** Magnetic resonance myocardial fiber-orientation mapping with direct

histological correlation. *Am J Physiol Heart Circ Physiol* 274: H1627–H1634, 1998.
21. **Josephson IR, Guia A, Stern MD, Lakatta EG.** Alterations in properties of L-type Ca channels in aging rat heart. *J Mol Cell Cardiol* 34: 297–308, 2002.
22. **Kannel WB, Cupples LA, D'Agostino RB.** Sudden death risk in overt coronary heart disease: the Framingham Study. *Am Heart J* 113: 799–804, 1987.
23. **Kingwell BA, Cameron JD, Gillies KJ, Jennings GL, Dart AM.** Arterial compliance may influence baroreflex function in athletes and hypertensives. *Am J Physiol Heart Circ Physiol* 268: H411–H418, 1995.
24. **Kondo T, Yamaki M, Kubota I, Tachibana H, Tomoike H.** Electrophysiologic effects of sodium channel blockade on anisotropic conduction and conduction block in canine myocardium: preferential slowing of longitudinal conduction by flecainide versus disopyramide or lidocaine. *J Am Coll Cardiol* 29: 1639–1644, 1997.
25. **Koura T, Hara M, Takeuchi S, Ota K, Okada Y, Miyoshi S, Watanabe A, Shiraiwa K, Mitamura H, Kodama I, Ogawa S.** Anisotropic conduction properties in canine atria analyzed by high-resolution optical mapping: preferential direction of conduction block changes from longitudinal to transverse with increasing age. *Circulation* 105: 2092–2098, 2002.
26. **Lakatta EG, Levy D.** Arterial and cardiac aging: Major shareholders in cardiovascular disease enterprises. Part II. The aging heart in health: Links to heart disease. *Circulation* 107: 346–354, 2003.
27. **Lantelme P, Khettab F, Custaud MA, Rial MO, Joanny C, Gharib C, Milon H.** Spontaneous baroreflex sensitivity: toward an ideal index of cardiovascular risk in hypertension? *J Hypertens* 20: 935–944, 2002.
28. **LeGrice IJ, Smaill BH, Chai LZ, Edgar SG, Gavin JB, Hunter PJ.** Laminar structure of the heart: ventricular myocyte arrangement and connective tissue architecture in the dog. *Am J Physiol Heart Circ Physiol* 269: H571–H582, 1995.
29. **Li Q, Wu S, Li SY, Lopez FL, Du M, Kajstura J, Anversa P, Ren J.** Cardiac-specific overexpression of insulin-like growth factor 1 attenuates aging-associated cardiac diastolic contractile dysfunction and protein damage. *Am J Physiol Heart Circ Physiol* 292: H1398–H1403, 2007.
30. **Lim CC, Liao R, Varma N, Apstein CS.** Impaired lusitropy-frequency in the aging mouse: role of Ca^{2+}-handling proteins and effects of isoproterenol. *Am J Physiol Heart Circ Physiol* 277: H2083–H2090, 1999.
31. **Mahmud A, Feely J.** Acute effect of caffeine on arterial stiffness and aortic pressure waveform. *Hypertension* 38: 227–231, 2001.
32. **Miller TR, Grossman SJ, Schectman KB, Biello DR, Ludbrook PA, Ehsani AA.** Left ventricular diastolic filling and its association with age. *Am J Cardiol* 58: 531–535, 1986.
33. **Mitchell GF.** Arterial Stiffness and Wave Reflection: Biomarkers of Cardiovascular Risk. *Artery Res* 3: 56–64, 2009.
34. **Mitchell GF, Hwang SJ, Vasan RS, Larson MG, Pencina MJ, Hamburg NM, Vita JA, Levy D, Benjamin EJ.** Arterial stiffness and cardiovascular events the Framingham Heart Study. *Circulation* 121: 505–511, 2010.
35. **Mitchell GF, Parise H, Benjamin EJ, Larson MG, Keyes MJ, Vita JA, Vasan RS, Levy D.** Changes in arterial stiffness and wave reflection with advancing age in healthy men and women - The Framingham Heart Study. *Hypertension* 43: 1239–1245, 2004.
36. **Mitchell GF, Pfeffer MA, Finn PV, Pfeffer JM.** Comparison of techniques for measuring pulse-wave velocity in the rat. *J Appl Physiol* 82: 203–210, 1997.
37. **Mitchell GF, Pfeffer MA, Westerhof N, Pfeffer JM.** Measurement of aortic input impedance in rats. *Am J Physiol Heart Circ Physiol* 267: H1907–H1915, 1994.
38. **Mitchell GF, Vasan RS, Keyes MJ, Parise H, Wang TJ, Larson MG, D'Agostino RB, Sr, Kannel WB, Levy D, Benjamin EJ.** Pulse pressure and risk of new-onset atrial fibrillation. *J Am Med Assoc* 297: 709–715, 2007.
39. **Mizumaki K, Fujiki A, Tani M, Misaki T.** Effects of acute ischemia on anisotropic conduction in canine ventricular muscle. *Pacing Clin Electrophysiol* 16: 1656–1663, 1993.
40. **Mortara A, Sleight P, Pinna GD, Maestri R, Prpa A, La Rovere MT, Cobelli F, Tavazzi L.** Abnormal awake respiratory patterns are common in chronic heart failure and may prevent evaluation of autonomic tone by measures of heart rate variability. *Circulation* 96: 246–252, 1997.
41. **Odening KE, Kirk M, Brunner M, Ziv O, Lorvidhaya P, Liu GX, Schofield L, Chaves L, Peng X, Zehender M, Choi BR, Koren G.** Electrophysiological studies of transgenic long QT type 1 and type 2 rabbits reveal genotype-specific differences in ventricular refractoriness and His conduction. *Am J Physiol Heart Circ Physiol* 299: H643–H655, 2010.
42. **Pacher P, Nagayama T, Mukhopadhyay P, Bátkai S, Kass DA.** Measurement of cardiac function using pressure-volume conductance catheter technique in mice and rats. *Nature Protocols* 3: 1422–1434, 2008.
43. **Rodeheffer RJ, Gerstenblith G, Becker LC, Fleg JL, Weisfeldt ML, Lakatta EG.** Exercise cardiac-output is maintained with advancing age in healthy-human subjects: cardiac dilatation and increased stroke volume compensate for a diminished heart-rate. *Circulation* 69: 203–213, 1984.
44. **Rogers WJ, Hu YL, Coast D, Vido DA, Kramer CM, Pyeritz RE, Reichek N.** Age-associated changes in regional aortic pulse wave velocity. *J Am Coll Cardiol* 38: 1123–1129, 2001.
45. **Rossi S, Baruffi S, Bertuzzi A, Miragoli M, Corradi D, Maestri R, Alinovi R, Mutti A, Musso E, Sgoifo A, Brisinda D, Fenici R, Macchi E.** Ventricular activation is impaired in aged rat hearts. *Am J Physiol Heart Circ Physiol* 295: H2336–H2347, 2008.
46. **Salata JJ, Jurkiewicz NK, Jow B, Folander K, Guinosso PJ Jr, Raynor B, Swanson R, Fermini B.** IK of rabbit ventricle is composed of two currents: evidence for IKs. *Am J Physiol Heart Circ Physiol* 271: H2477–H2489, 1996.
47. **Schatzkin A, Cupples LA, Heeren T, Morelock S, Kannel WB.** Sudden-death in the Framingham Heart-Study: differences in incidence and risk-factors by sex and coronary-disease status. *Am J Epidemiol* 120: 888–899, 1984.
48. **Schmidlin O, Bharati S, Lev M, Schwartz JB.** Effects of physiological aging on cardiac electrophysiology in perfused Fischer 344 rat hearts. *Am J Physiol Heart Circ Physiol* 262: H97–H105, 1992.
49. **Schmidt U, del Monte F, Miyamoto MI, Matsui T, Gwathmey JK, Rosenzweig A, Hajjar RJ.** Restoration of diastolic function in senescent rat hearts through adenoviral gene transfer of sarcoplasmic reticulum Ca(2+)-ATPase. *Circulation* 101: 790–796, 2000.
50. **Schulman SP, Lakatta EG, Fleg JL, Lakatta L, Becker LC, Gerstenblith G.** Age-related decline in left-ventricular filling at rest and exercise. *Am J Physiol Heart Circ Physiol* 263: H1932–H1938, 1992.
51. **Scollan DF, Holmes A, Winslow R, Forder J.** Histological validation of myocardial microstructure obtained from diffusion tensor magnetic resonance imaging. *Am J Physiol Heart Circ Physiol* 275: H2308–H2318, 1998.
52. **Slack JP, Grupp IL, Dash R, Holder D, Schmidt A, Gerst MJ, Tamura T, Tilgmann C, James PF, Johnson R, Gerdes AM, Kranias EG.** The enhanced contractility of the phospholamban-deficient mouse heart persists with aging. *J Mol Cell Cardiol* 33: 1031–1040, 2001.
53. **Stein M, Boulaksil M, Jansen JA, Herold E, Noorman M, Joles JA, van Veen TA, Houtman MJ, Engelen MA, Hauer RN, de Bakker JM, van Rijen HV.** Reduction of fibrosis-related arrhythmias by chronic renin-angiotensin-aldosterone system inhibitors in an aged mouse model. *Am J Physiol Heart Circ Physiol* 299: H310–H321, 2010.
54. **Stein M, Noorman M, van Veen TA, Herold E, Engelen MA, Boulaksil M, Antoons G, Jansen JA, van Oosterhout MF, Hauer RN, de Bakker JM, van Rijen HV.** Dominant arrhythmia vulnerability of the right ventricle in senescent mice. *Heart Rhythm* 5: 438–448, 2008.
55. **Taneja T, Mahnert BW, Passman R, Goldberger J, Kadish A.** Effects of sex and age on electrocardiographic and cardiac electrophysiological properties in adults. *Pacing Clin Electrophysiol* 24: 16–21, 2001.
56. **Tsuboi N, Kodama I, Toyama J, Yamada K.** Anisotropic conduction properties of canine ventricular muscles. Influence of high extracellular K+ concentration and stimulation frequency. *Jpn Circ J* 49: 487–498, 1985.
57. **Varro A, Lathrop DA, Hester SB, Nanasi PP, Papp JG.** Ionic currents and action potentials in rabbit, rat, and guinea pig ventricular myocytes. *Basic Res Cardiol* 88: 93–102, 1993.
58. **Walker KE, Lakatta EG, Houser SR.** Age associated changes in membrane currents in rat ventricular myocytes. *Cardiovasc Res* 27: 1968–1977, 1993.
59. **Xu A, Narayanan N.** Effects of aging on sarcoplasmic reticulum Ca2+-cycling proteins and their phosphorylation in rat myocardium. *Am J Physiol Heart Circ Physiol* 275: H2087–H2094, 1998.
60. **Yershov AL, Jordan BS, Fudge JM, Dubick MA.** Influence of the mode of ventilation on ketamine/xylazine requirements in rabbits. *Vet Anaesth Analg* 34: 157–163, 2007.
61. **Zheng ZJ, Croft JB, Giles WH, Mensah GA.** Sudden cardiac death in the United States, 1989 to 1998. *Circulation* 104: 2158–2163, 2001.
62. **Zhu X, Altschafl BA, Hajjar RJ, Valdivia HH, Schmidt U.** Altered Ca2+ sparks and gating properties of ryanodine receptors in aging cardiomyocytes. *Cell Calcium* 37: 583–591, 2005.
63. **Zipes DP, Jalife editors J.** *Cardiac Electrophysiology: From Cell to Bedside*. Philadelphia, PA: Saunders, 1990, p. 353–364.